



Optics Letters

SNAP microwave optical filters

M. SUMETSKY 

Aston Institute of Photonic Technologies, Aston University, Birmingham B4 7ET, UK (m.sumetsky@aston.ac.uk)

Received 1 June 2021; revised 8 July 2021; accepted 21 July 2021; posted 22 July 2021 (Doc. ID 433077); published 20 August 2021

If the originally flat bottom of a wide quantum well with multiple eigenstates is periodically modulated, its eigenvalues rearrange into denser groups separated by wider gaps. We show that this effect, if implemented in an elongated bottle microresonator [also called a surface nanoscale axial photonics (SNAP) microresonator] allows us to design microwave photonic tunable filters with an outstanding performance.

Published by The Optical Society under the terms of the [Creative Commons Attribution 4.0 License](https://creativecommons.org/licenses/by/4.0/). Further distribution of this work must maintain attribution to the author(s) and the published article's title, journal citation, and DOI.

<https://doi.org/10.1364/OL.433077>

Design and fabrication of high-quality microwave filters is a longstanding problem that has attracted scientists and engineers for several decades [1–3]. The interest in this problem is motivated by critical applications of microwave filters in modern communication technologies, where their accurate transmission spectrum characteristics are highly desirable to combine with small dimensions and broadband tunability. Photonics suggests several solutions to this problem based on miniature photonic circuits [4–6]. In particular, much research work was done to design and fabricate microwave filters based on coupled ring resonators [7–9], photonic crystals [10], distributed feedback resonators [11], Mach–Zehnder interferometers [12], fiber Bragg gratings [13], frequency comb generators [14], Brillouin scattering [15], and other approaches [4–6].

In many cases, it is important to create filters in which transmission amplitude has a maximum flatness within the predetermined bandwidth and steeply vanishes outside it. Theoretically, filters with predetermined flatness and high rejection rate can be designed by apodization of coupled microresonator circuits with a sufficiently large number of elements [16,17]. Experimentally, the intrinsic losses and insufficient fabrication precision lead to severe noise in the transmission amplitude of such circuits growing with the number of resonant elements [18] and impracticality of devices fabricated of sufficiently large number of coupled microresonators.

Even for negligible propagation losses, at light frequency f and for the pass bandwidth Δf , microresonators with characteristic dimension d should be fabricated with the precision of better than $\Delta d \sim \Delta f d / f$. For characteristic $f = 200$ THz, $\Delta f = 100$ MHz, and $d = 100$ μm , we have $\Delta d \sim 0.5$ \AA , which is not possible to achieve by conventional modern microphotonic fabrication technologies. For this reason,

coupled ring resonators and other photonic infinite impulse response filters were fabricated with the aid of microheaters, enabling us to tune the circuit elements individually (see, e.g., [9,11,19] and references therein).

Increasing the microresonator Q -factor allows us to create filters with better passband flatness and larger rejection rate. Indeed, at optical frequency f , the pass bandwidth cannot be smaller than $\Delta f_{\text{pass}} \sim f / Q$, while to arrive at sufficient flatness we have to have $Q \gg f / \Delta f_{\text{pass}}$. Thus, at $f = 200$ THz, the characteristic for microwave applications passband with $\Delta f_{\text{pass}} = 100$ MHz requires $Q \gg 2 \cdot 10^6$. That high and much higher Q -factors are possible to achieve in stand-alone microresonators [20,21]. However, the problem of effectively combining them into a circuit of multiple elements with the predetermined dimensions and coupling remains open.

Favorably, the ultraprecise fabrication precision combined with ultralow material and scattering losses required for realization of microwave photonic filters can be achieved in the surface nanoscale axial photonics (SNAP) technology [22–26], which has not yet been considered for microwave applications. In SNAP, the required microresonator circuits are fabricated in the form of coupled bottle microresonators having nanoscale effective radius variation (ERV). In Ref. [23], 30 coupled bottle microresonators were fabricated at the surface of a 19 μm radius optical fiber with better than 1 \AA precision. In Ref. [25], it was shown that coupled SNAP bottle microresonators can be post-processed with the frequency precision of better than 0.2 GHz. This fabrication precision can be further improved since in Ref. [25] it was limited by the resolution of the optical spectrum analyzer used. The intrinsic Q -factor of bottle microresonators (characterizing material and scattering losses) can be greater than the loaded Q -factor $3 \cdot 10^8$ of a bottle resonator with similar radius measured in Ref. [27]. All of this suggests the SNAP technology as a promising approach for fabrication of practical microwave photonics filters and signal processing devices.

In this Letter, we consider a SNAP microresonator (SMR) with periodically modulated ERV illustrated in Fig. 1(a) (which can be also considered as a system of coupled bottle microresonators) coupled to the input microfiber MF1 and output microfiber MF2. The frequency eigenvalue structure of this SMR is illustrated in Fig. 1(b). This structure has a series of dense eigenfrequencies separated from others by a gap. The experimental realization of similar SMRs with subangstrom precision was demonstrated in [22,23], while a four-port resonant SMR device coupled to two microfibers was fabricated in Ref. [28] following the demonstration of an ultralow loss four-port microtoroid device in Ref. [29]. We show that below that

the periodic SMR structure illustrated in Fig. 1 can be apodized and appropriately coupled to MF1 and MF2 to perform as a bandpass filter with close to flat transmission amplitude and high rejection.

Following the SNAP theory [22], we consider whispering gallery modes (WGMs), which slowly propagate along the SMR axis z and introduce the cutoff frequency $f_c(z)$ corresponding to a WGM with fixed azimuthal and axial quantum numbers, $m = m_0$ and $p = p_0$. A relatively small nonresonant transmission from MF1 to MF2 determined by WGMs with other quantum numbers, which limits the rejection rate, will be discussed later. The nanoscale ERV $\Delta r(z) = r(z) - r_0$ of a SMR with radius r_0 is expressed through the cutoff frequency variation (CFV) $\Delta f_c(z) = f_c(z) - f_0$ as $\Delta r(z) = r_0 \Delta f_c(z) / f_0$. Therefore, we can characterize a SMR either by ERV $\Delta r(z)$ or by CFV $\Delta f_c(z)$. We also introduce the frequency variation $\Delta f = f - f_0$ and characteristic frequency variation of our SMR Δf_0 [Fig. 1(b)]. Then, the one-dimensional wave equation describing the axial dependence of WGM amplitude [22] can be presented in the dimensionless form:

$$\Psi_{\zeta\zeta} + (\varepsilon - \nu(\zeta) + i\gamma + \Lambda\delta(\zeta - \zeta_{MF}) + \Lambda\delta(\zeta + \zeta_{MF})) \Psi = 0. \quad (1)$$

Here, the dimensionless frequency ε , attenuation γ , MF-SMR coupling parameter Λ , and distance along the SMR ζ are defined as

$$\varepsilon = \frac{\Delta f}{\Delta f_0}, \quad \gamma = \frac{g}{\Delta f_0}, \quad \zeta = \frac{z}{z_0}, \quad \Lambda = z_0 D, \quad (2)$$

$$z_0 = \frac{\pi c}{2^{3/2} n(f_0 \Delta f_0)^{1/2}},$$

where c is the speed of light, n is the SMR refractive index (below we consider silica SMR with $n = 1.44$), g is the attenuation expressed through its Q -factor as $g = f_0/Q$, and D is the microfiber-SMR complex-valued coupling parameter [22], which is assumed to be the same for MF1 and MF2. We also assume that the SMR is symmetric with respect to its center at $z = 0$, and MF1 and MF2 are positioned symmetrically at axial coordinates $z = z_{MF}$ and $z = -z_{MF}$. Then, provided that the microfiber-SMR coupling is lossless [29,30], the transmission amplitude $S_{12}(f, z_{MF})$ from MF1 to MF2 is determined as [22]

$$S_{12}(\Delta f, z_{MF}) = \frac{2 \operatorname{Im}(\Lambda) G(\varepsilon, \zeta_{MF}, -\zeta_{MF})}{(1 + \Lambda G(\varepsilon, \zeta_{MF}, \zeta_{MF}))^2 - \Lambda^2 G^2(\varepsilon, \zeta_{MF}, -\zeta_{MF})}. \quad (3)$$

Here, $\zeta_{MF} = z_{MF}/z_0$, $\varepsilon = \Delta f/\Delta f_0$ and $G(\varepsilon, \zeta_1, \zeta_2)$ is the Green's function of Eq. (1). To take into account the coupling loss (which can be very small for a four-port microresonator [29]), the numerator in this equation should be reduced accordingly [22,28]. The dimensionless form of Eqs. (1)–(3) allows us to design filters with different passbands Δf_{pass} by rescaling. It follows from Eqs. (2) and (3) that to design a filter with passband $\sigma \Delta f_{\text{pass}}$ from a filter with passband Δf_{pass} we have to rescale the CFV of the last filter by σ , its length by $\sigma^{-1/2}$, its Q -factor by σ , and the coupling parameter D by $\sigma^{1/2}$.

We start with the design of a 100 MHz passband filter constructed of four coupled microresonators modeled by harmonic oscillations of CFV plotted in Fig. 2(a). Fabrication of similar SMR with subangstrom precision was demonstrated in [22,23]. The CFV precision achieved in [25] was 0.16 GHz, sufficient to introduce the CFV with characteristic 2 GHz amplitude shown in Fig. 2(a). In our modeling, we assume that the intrinsic SMR Q -factor, which determines its internal losses, is $Q = 10^8$ [27,31] and set the frequency $f_0 = 193.4$ THz corresponding to the center of optical communication C-band of 1550 nm. We optimize the symmetric positions of MF1 and MF2 to arrive at the best flat transmission power $|S_{12}|^2$ within bandwidth $\Delta f_{\text{pass}} = 100$ MHz and vanishing outside it. The result of optimization is shown in Fig. 2(b) along the whole SMR spectrum and in Fig. 2(c) for the spectrum in the vicinity of the passband considered. It is seen that the transmission power is quite flat within the passband and vanishes down to -100 dB in its vicinity (we show below that this value can be prevailed by nonresonant transmission). The optimized positions of MF1 and MF2 are $\pm z_{\text{opt}} = \pm 381 \mu\text{m}$, and the coupling parameter is $D = 0.0015 + 0.0017i \mu\text{m}^{-1}$. This value of D is an order of magnitude less than those typically observed for the coupling of the microfiber and SMR positioned in direct contact [22,23,32]. We suggest that this small coupling can be achieved by bending the microfiber [7] or placing it (or a planar waveguide) several hundred nanometers away from the SMR [30]. Remarkably, we found that the displacement of MF1 and MF2 by several microns followed by optimization of D does not significantly change the behavior of $|S_{12}|^2$.

Increasing the number of coupled microresonators and apodization of their initially periodic ERV allows us to add more flexibility in designing a filter and achieve better passband flatness and rejection rate. In the next example, we design a 1 GHz passband filter by optimization of an SMR composed of eight coupled microresonators. Now, in addition to the optimization of positions of MF1 and MF2 made above, we apodize the SMR by narrowing the barriers between the first, second, and third and, symmetrically, between the sixth, seventh, and eighth microresonators. The optimized CFV of a SMR with the Q -factor $Q = 10^8$ is plotted in Fig. 3(a). While narrowing of the barriers is achieved here by straightforward cutting, we suggest that, in a more advanced CFV optimization, the barrier widths can be adjusted in a way more suitable for experimental realization. It is seen from Fig. 3(a) that the length of the designed 1 GHz filter is much smaller than that of the 100 MHz

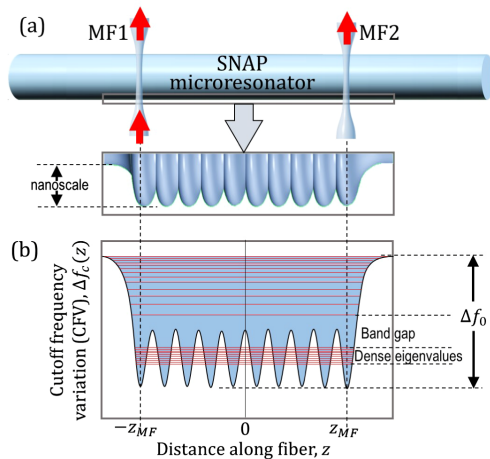


Fig. 1. (a) Illustration of a SMR with nanoscale periodically modulated ERV coupled to microfibers MF1 and MF2 and (b) the corresponding CFV. Red lines are the axial frequency eigenvalues of SMR.

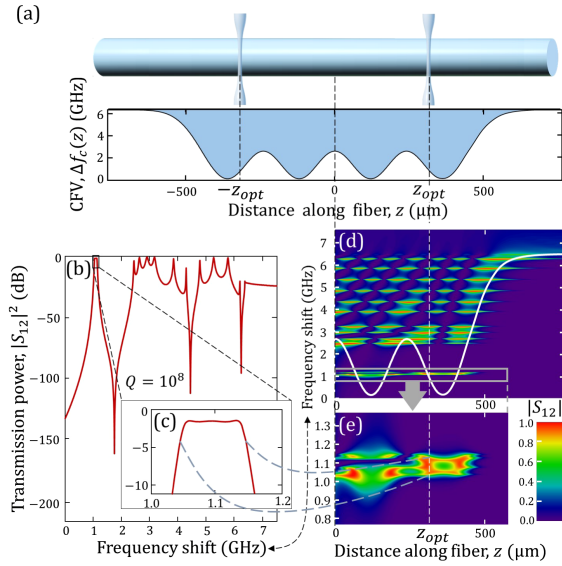


Fig. 2. (a) CFV for a SMR consisting of four coupled microresonators. (b) Transmission power spectrum of optimized SMR along its whole bandwidth and (c) near the passband considered. (d) Spectrogram of transmission amplitude $|S_{12}|$ calculated for the optimized coupling parameter D , which is magnified near the considered passband in (e).

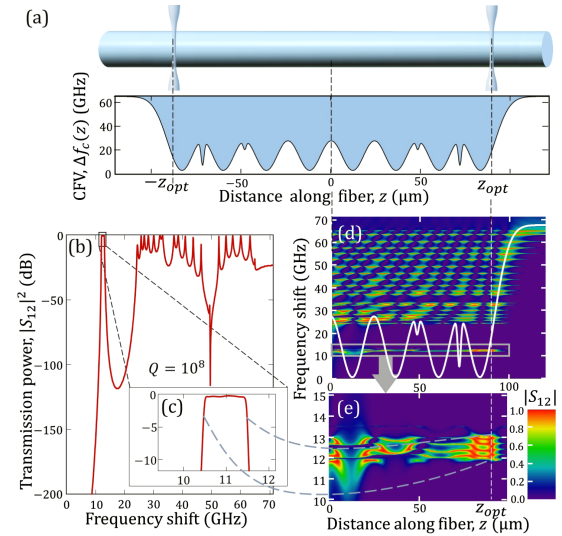


Fig. 3. (a) CFV for a SMR consisting of eight coupled microresonators. (b) Transmission power spectrum of optimized SMR along its whole bandwidth and (c) near the passband considered. (d) Spectrogram of transmission amplitude $|S_{12}|$ calculated for the optimized coupling parameter D , which is magnified near the considered passband in (e).

filter shown in Fig. 2, and its CFV is much greater. Figure 3(b) shows the spectrum of the transmission power $|S_{12}|^2$ along the full SMR bandwidth, which was obtained by optimization of the transmission power along the passband magnified in Fig. 3(c). The determined optimized positions of MF1 and MF2 are $\pm z_{\text{opt}} = \pm 90 \mu\text{m}$, and the coupling parameter is $D = 0.0145 + 0.013i \mu\text{m}^{-1}$.

The considered models and rescaling relations indicated above allow us to design SMRs having CFVs and transmission spectra with other passbands. For example, to design a SMR with 500 MHz passband from the 100 MHz passband SMR with $Q = 10^8$ described above (Fig. 2), we have to magnify the frequency values along the horizontal axis in Figs. 2(b) and 2(c) by five. The CFV of this SMR is obtained by dividing the values of distance along the horizontal axis in Fig. 2(a) by $5^{1/2}$ (i.e., this SMR is $5^{1/2}$ times shorter) and multiplying the CFV values along the vertical axis by five. The Q -factor of this SMR is five times smaller, $Q = 2 \cdot 10^7$.

The calculated very large transmission sideband rejection [down to -100 dB in both cases shown in Figs. 2(b) and 3(b)] can be violated by nonresonant transmission of light from MF1 to MF2 not taken into account by Eq. (1), which describes the contribution of WGMs having a single azimuthal and radial quantum number, $m = m_0$ and $p = p_0$, only. To estimate the contribution of WGMs with nonresonant quantum numbers greater than $p = 0$ vanish (like, e.g., in a capillary SMR with sufficiently narrow walls [33]). We introduce the separation of the cutoff frequencies Δf_{az} along the azimuthal quantum number m in the vicinity $|\Delta m| \ll m_0$ of m_0 , where $\Delta m = m_0 - m$. Then, Δf_{az} is expressed through the SMR radius r_0 as $\Delta f_{az} = c(2\pi nr_0)^{-1}$. For fiber radii and CFVs of our concern, $r_0 \lesssim 1 \text{ mm}$ and $\Delta f_0 \lesssim 10 \text{ GHz}$, we have $\Delta f_0 \ll \Delta f_{az}$. Under these assumptions, the contribution to the nonresonant transmission $S_{12}^{(nr)}$ of azimuthal modes with $\Delta m < 0$ is negligible, while the contribution of M WGMs with $\Delta m > 0$ is [34]

$$S_{12}^{(nr)} = S_0^{(nr)} \Xi,$$

$$\Xi = \sum_{\Delta m=1}^M \frac{1}{\Delta m^{1/2}} \exp \left[2i\beta_{az} z_{\text{opt}} \left(\Delta m + \frac{\Delta f}{\Delta f_{az}} \right)^{1/2} \right],$$

$$S_0^{(nr)} = \frac{\text{Im}(D)}{\beta_{az}},$$

$$\beta_{az} = \frac{2^{2/3} \pi n}{c} (f_0 \Delta f_{az})^{1/2}, \quad \Delta f_{az} = \frac{c}{2\pi nr_0}. \quad (4)$$

Factor $S_0^{(nr)}$ in this equation determines the characteristic value of nonresonance transmission, while the sum over Δm rapidly oscillates as a function of SMR radius r_0 . For the 100 MHz passband SMR considered above (Fig. 2) with radius $r_0 = 20 \mu\text{m}$, we have $20 \log(S_0^{(nr)}) \cong -53 \text{ dB}$. For the 1 GHz filter with the same radius (Fig. 3), we have $20 \log(S_0^{(nr)}) \cong -35 \text{ dB}$. These values are much greater than the rejection rates calculated above in the resonance approximation. Therefore, they determine the sideband rejection rate of the designed filters. The increase of the rejection rate with the reduction of microfiber-SMR coupling determined by $\text{Im}(D)$ correlates with experimental observations for a ring microresonator [35]. Numerical modeling based on Eq. (4) shows that these sideband transmission values can be reduced by $\sim 10 \text{ dB}$ by optimization of the fiber radius r_0 . Much better reduction of the nonresonant transmission can be achieved by appropriate

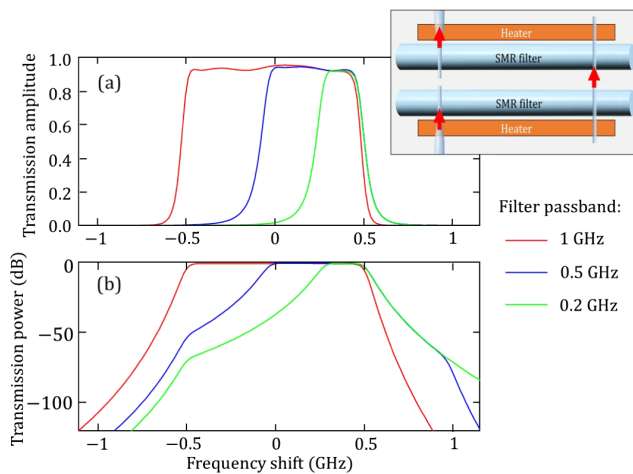


Fig. 4. (a) Tunable filter comprised of two 1 GHz filters connected in series. (b) Transmission filter power spectra of this filter tuned to 1 GHz, 0.5 GHz, and 0.2 GHz passbands. (c) Same spectra magnified near the passbands.

bending of the microfiber around the SMR, which results in the phase matching [7,36] to be considered elsewhere.

Remarkably, connection of SMR filters in series allows us to significantly reduce the nonresonant transmission in the rejection region and achieve the passband tunability. As an example, we consider a device consisting of two SMR 1 GHz passband filters designed above connected in series, as illustrated in Fig. 4(a). The transmission amplitude of this filter is found as $S_{12}^{(2)} = S_{12}(\Delta f - \Delta f_{sh1}, z_{MF}) S_{12}(\Delta f - \Delta f_{sh2}, z_{MF})$. Here, $\Delta f_{sh1,2}$ are the shifts of the cutoff frequencies of SMRs, which can be tuned by adjacent thermal heaters shown in Fig. 4(a). This allows us to tune both the central frequency and the passband width of the filter. Figures 4(b) and 4(c) show the spectra of transmission power of this filter for $\Delta f_{sh1} = 0$ and $\Delta f_{sh2} = 0$ (1 GHz passband, red curves), $\Delta f_{sh2} = 0.5$ GHz (0.5 GHz passband, blue curves), and $\Delta f_{sh2} = 0.8$ GHz (0.2 GHz passband, green curves). The estimated rejection rate limited by the nonresonant transmission with the amplitude $S_0^{(nr)}$ defined by Eq. (4) is now ~ 70 dB.

We suggest that optimization of a SMR profile with more flexible CFV parameters, as well as SMRs connected in series, will lead to filter designs with superior transmission characteristics. Experimentally, optimization of the MF1 and MF2 positions and their coupling to SMR can be performed by their translation along the microfiber and SMR directions [24], bending [7,36], and by tuning the microfiber-SMR gap [30]. Finally, the design and experimental realization of SMR devices for more general microwave photonics spectral shaping [37] may be of special interest.

Funding. Engineering and Physical Sciences Research Council (EP/P006183/1).

Disclosures. The author declares no conflicts of interest.

Data Availability. Data underlying the results presented in this Letter are not publicly available at this time but may be obtained from the authors upon reasonable request.

REFERENCES AND NOTE

- L. Zhu, S. Sun, and R. Li, *Microwave Bandpass Filters for Wideband Communications* (Wiley, 2012).
- R. J. Cameron, C. M. Kudsia, and R. R. Mansour, *Microwave Filters for Communication Systems: Fundamentals, Design, and Applications*, 2nd ed. (Wiley, 2018).
- H. Islam, S. Das, T. Bose, and T. Ali, *IEEE Access* **8**, 185429 (2020).
- D. Marpaung, J. Yao, and J. Capmany, *Nat. Photonics* **13**, 80 (2019).
- Y. Liu, A. Choudhary, D. Marpaung, and B. J. Eggleton, *Adv. Opt. Photon.* **12**, 485 (2020).
- G. Serafino, S. Maresca, C. Porzi, F. Scotti, P. Ghelfi, and A. Bogoni, *J. Lightwave Technol.* **38**, 5339 (2020).
- B. E. Little, S. T. Chu, H. A. Haus, J. Foresi, and J.-P. Laine, *J. Lightwave Technol.* **15**, 998 (1997).
- W. Bogaerts, P. De Heyn, T. Van Vaerenbergh, K. De Vos, S. K. Selvaraja, T. Claes, P. Dumon, P. Bienstman, D. Van Thourhout, and R. Baets, *Laser Photon. Rev.* **6**, 47 (2012).
- T. A. Huffman, G. M. Brodnik, C. Pinho, S. Gundavarapu, D. Baney, and D. J. Blumenthal, *IEEE J. Sel. Top. Quantum Electron.* **24**, 5900209 (2018).
- J. Sancho, J. Bourderionnet, J. Lloret, S. Combr e, I. Gasulla, S. Xavier, S. Sales, P. Colman, G. Lehoucq, D. Dolfi, J. Capmany, and A. De Rossi, *Nat. Commun.* **3**, 1075 (2012).
- C. Porzi, G. J. Sharp, M. Sorel, and A. Bogoni, *IEEE J. Quantum Electron.* **56**, 6500109 (2020).
- E. J. Norberg, R. S. Guzzon, J. S. Parker, L. A. Johansson, and L. A. Coldren, *J. Lightwave Technol.* **29**, 1611 (2011).
- C. Wang and J. Yao, *Opt. Express* **21**, 22868 (2013).
- M. Tan, X. Xu, J. Wu, R. Morandotti, A. Mitchell, and D. J. Moss, *Opt. Commun.* **465**, 125563 (2020).
- Y. Xie, A. Choudhary, Y. Liu, D. Marpaung, K. Vu, P. Ma, D.-Y. Choi, S. Madden, and B. J. Eggleton, *J. Lightwave Technol.* **37**, 5246 (2019).
- M. Sumetsky and B. J. Eggleton, *Opt. Express* **11**, 381 (2003).
- H.-C. Liu and A. Yariv, *Opt. Express* **19**, 17653 (2011).
- W. Bogaerts, M. Fiers, and P. Dumon, *IEEE J. Sel. Top. Quantum Electron.* **20**, 8202008 (2014).
- A. A. Savchenkov, V. S. Ilchenko, A. B. Matsko, and L. Maleki, *IEEE Photon. Technol. Lett.* **17**, 136 (2005).
- D. V. Strekalov, C. Marquardt, A. B. Matsko, H. G. L. Schwefel, and G. Leuchs, *J. Opt.* **18**, 123002 (2016).
- L. Wu, H. Wang, Q. Yang, Q. Ji, B. Shen, C. Bao, M. Gao, and K. Vahala, *Opt. Lett.* **45**, 5129 (2020).
- M. Sumetsky, *Opt. Express* **20**, 22537 (2012).
- M. Sumetsky and Y. Dulashko, *Opt. Express* **20**, 27896 (2012).
- M. Sumetsky, *Phys. Rev. Lett.* **111**, 163901 (2013).
- N. A. Toropov and M. Sumetsky, *Opt. Lett.* **41**, 2278 (2016).
- Q. Yu, Z. Zhang, and X. Shu, *Opt. Lett.* **46**, 1005 (2021).
- M. P llinger, D. O'Shea, F. Warken, and A. Rauschenbeutel, *Phys. Rev. Lett.* **103**, 053901 (2009).
- M. Crespo-Ballesteros, Y. Yang, N. Toropov, and M. Sumetsky, *Opt. Lett.* **44**, 3498 (2019).
- H. Rokhsari and K. J. Vahala, *Phys. Rev. Lett.* **92**, 253905 (2004).
- S. M. Spillane, T. J. Kippenberg, O. J. Painter, and K. J. Vahala, *Phys. Rev. Lett.* **91**, 043902 (2003).
- M. L. Gorodetsky, A. D. Pryamikov, and V. S. Ilchenko, *J. Opt. Soc. Am. B* **17**, 1051 (2000).
- D. L. P. Vitullo, S. Zaki, D. E. Jones, M. Sumetsky, and M. Brodsky, *Opt. Express* **28**, 25908 (2020).
- G. Gardosi, B. J. Mangan, G. S. Puc, and M. Sumetsky, *ACS Photon.* **8**, 436 (2021).
- Equation (4) is found by generalization of Eq. (A1.7) of Ref. [22] by adding terms determined by Green's functions with $m \neq m_0$ from Eq. (A1.3) of Ref. [22]. The expression for these Green's functions are given by Eq. (17) of the same reference. We also assume that the coupling parameter D for the WGMs with m close to m_0 is the same.
- H. Qiu, F. Zhou, J. Qie, Y. Yao, X. Hu, Y. Zhang, X. Xiao, Y. Yu, J. Dong, and X. Zhang, *J. Lightwave Technol.* **36**, 4312 (2018).
- B. E. Little, J.-P. Laine, and H. A. Haus, *J. Lightwave Technol.* **17**, 704 (1999).
- O. Daulay, G. Liu, X. Guo, M. Eijkel, and D. Marpaung, *J. Lightwave Technol.* **39**, 700 (2021).